Bell pepper yield estimation using time series unmanned air vehicle multispectral vegetation indexes and canopy volume

Article *in* Journal of Applied Remote Sensing · March 2022

DOI: 10.1117/1.JRS.16.022202

2 authors:

Emre Tunca
Duzce University
16 PUBLICATIONS **62** CITATIONS

SEE PROFILE

Eyup Selim Koksal
Ondokuz Mayıs Üniversitesi
45 PUBLICATIONS **437** CITATIONS

SEE PROFILE

Bell pepper yield estimation using time series unmanned air vehicle multispectral vegetation indexes and canopy volume

Emre Tunca* **and Eyüp Selim Köksal**
Ondokuz Mayıs University, Department of Agricultural Structures and Irrigation, Agriculture Faculty, Samsun, Turkey

Abstract. Accurate and timely crop yield estimation prior to harvest is important for agricultural management, agricultural economy, and food security. In many cases, the farmers estimate the yield visually. Further, several crop simulation models have been developed to estimate yield accurately. However, these are not used efficiently because of their requirements for enormous amounts of data and their inability to show the spatial differences of yield in the field. Recently, the rapid development of unmanned air vehicle (UAV) technologies has shown great potential to estimate crop yield accurately and show the spatial heterogeneity in the field. We estimate the bell pepper yield with time series, high-resolution UAV multispectral images. To do so, canopy volume and five different spectral vegetation indices used widely were calculated. Seven UAV flight missions were conducted between June and August of 2019. Various linear regression models were developed to estimate the bell pepper yield based on the canopy volume values and vegetation indices. The results showed that the bell pepper canopy volume fit the yield best with the minimum estimation error [coefficient of determination $(R^2) = 0.93$ and root mean square error $(\mathrm{RMSE}) = 2.30$ tons ha^{-1}]. In addition, a significant correlation was found between the enhanced vegetation index and bell pepper yield ($R^2 = 0.87$ and $\mathrm{RMSE} = 3.16$ tons ha^{-1}). © *2022 Society of Photo-Optical Instrumentation Engineers (SPIE)* [DOI: 10.1117/1.JRS.16.022202]

Keywords: bell pepper yield; unmanned air vehicle; multispectral image; vegetation index; canopy volume; enhanced vegetation index.

Paper 210533SS received Aug. 21, 2021; accepted for publication Dec. 8, 2021; published online Mar. 7, 2022.

1 Introduction

Vegetables are essential for human health and nutrition because of their high protein, carbohydrate, enzyme, vitamin, and mineral content.[1] Given the global population growth rate, the production of a greater quantity of vegetables of higher quality is necessary to ensure food security. Therefore, a robust solution is needed to prevent interannual fluctuations in yield, and monitoring vegetable farms to schedule irrigation and fertilizer and pesticide application is vital to ensure adequate yields.

Remote sensing (RS)-based monitoring tools are used widely in cartography,[2] geology,[3] ecology,[4] forestry,[5] and agriculture.[6] In the past two decades, RS has become a prominent tool for monitoring crops in agriculture as well.[7] RS allows rapid, inexpensive, and nondestructive vegetation monitoring.[8] In this context, significant research results on RS techniques' use have been reported related to vegetation monitoring,[9] evapotranspiration mapping,[10] and estimation of crop biophysical parameters, such as height,[11] biomass,[12] and yield.[13] Recently, yield estimation has become an important issue for those who make decisions about agricultural policy, food security, agricultural economy, and insurance. For instance, the regional winter wheat yield in China was estimated using MODIS satellite images.[14] Further, to reach a target profit, farmers need to estimate the amount of yield before harvest to schedule agricultural treatments, such as fertilization, irrigation, and pest control.

*Address all correspondence to Emre Tunca, emre.tunca@omu.edu.tr

1931-3195/2022/$28.00 © 2022 SPIE

Traditionally, farmers evaluate crop yield based on their experiences, field observations, and/or plant samples taken from specific regions in their fields. In addition, yield can be estimated before the harvest using the statistical relation between agrometeorological parameters and crop properties[15] and various crop models.[16] However, yield can vary from one point to another within a field depending upon the variation in soil physical and chemical properties, irrigation and fertilization scheduling and uniformity, the distribution of diseases and pests, and the effectiveness of chemical application against them. Within this framework, point scale yield estimation approaches do not consider spatial differences in the field, while RS can show spatial and temporal vegetation differences in the field.[17] As a result, yield can be estimated using these more efficient and precise RS techniques.

Some studies have shown that yield can be estimated successfully using satellite[18] and manned aircraft[19] systems. However, satellite images have some limitations attributable to their spatial and temporal resolution and the quality of images acquired under cloudy conditions. Although images with high spatial and temporal resolution can be obtained with manned aircraft, these platforms cannot be used for small-scale farmland because of the mission's high cost.[20]

To fill this gap, unmanned air vehicle (UAV) systems have been developed to acquire images with high spatial and temporal resolution.[21] A UAV is a type of aircraft with high maneuverability that can fly autonomously or with a remote controller.[22] As sensor technology has advanced, the weight of remote sensors has decreased, and thus, most UAVs are able to carry these sensors. Accordingly, this RS platform has become one of the crucial alternatives to other such platforms to monitor crop cultivation areas. In a study Ref. 23 conducted, normalized difference vegetation index (NDVI) values obtained from images, from satellites, manned aircraft, and UAV systems, were compared. The authors concluded that UAVs can be used to monitor small-scale fields efficiently. They also indicated that UAV images can show spatial differences better than satellite images can. In another study, mango yield was estimated successfully [coefficient of determination (R^2) greater than 0.77 and root mean square error (RMSE) (%) values that ranged between 20% and 29%] using high-resolution UAV multispectral images.[24] In addition to these studies, other research has been conducted on different crops, such as cotton,[13] rice,[25] grapes,[26] maize,[27] sugarcane,[28] soybean,[29] barley,[30] rapeseed,[31] and sunflower.[17] In recent years, many studies have used machine learning algorithms to estimate crop yield. For example, Ref. 13 combined three different machine learning algorithms (random forest, support vector machine, and K-nearest neighbors) to estimate alfalfa yield. Their results showed that an ensemble model estimated alfalfa yield accurately ($R^2 = 0.87$). Reference 32 estimated potato yield using UAV-based RGB and hyperspectral images and a random forest regression model ($R^2 = 0.63$). In addition, Refs. 29 and 30 used a deep learning approach successfully in barley (accuracy greater than 83%) and soybean ($R^2 = 0.70$), respectively. Further, some researchers have combined a crop growth model and RS-based data. For example, Ref. 33 estimated sugarcane yield by integrating plant height values into the soil–water–atmosphere–plant model, whereas Ref. 34 estimated wheat leaf area index from UAV point cloud data, after which these values were used in the SAFY model to estimate wheat yield.

The main objective of this study was to explore the use of high-resolution UAV multispectral images to estimate bell pepper yield during the growing period. The specific goals of this study were (1) to evaluate the UAV based high-resolution multispectral images' ability to monitor bell pepper during the growing season, (2) to compare the performance of vegetation indices and canopy volume on different dates to estimate bell pepper yield, and (3) to test the robustness of the bell pepper yield estimation model.

2 Materials and Methods

2.1 *Study Area*

The study area (41°36′09.17″, altitude 15 m above sea level) was located at the Soil and Water Resources Research Center of the Black Sea Agricultural Research Institute in the county of Bafra, Samsun, Turkey (Fig. 1). The study area's climate is characterized as subhumid.[35]

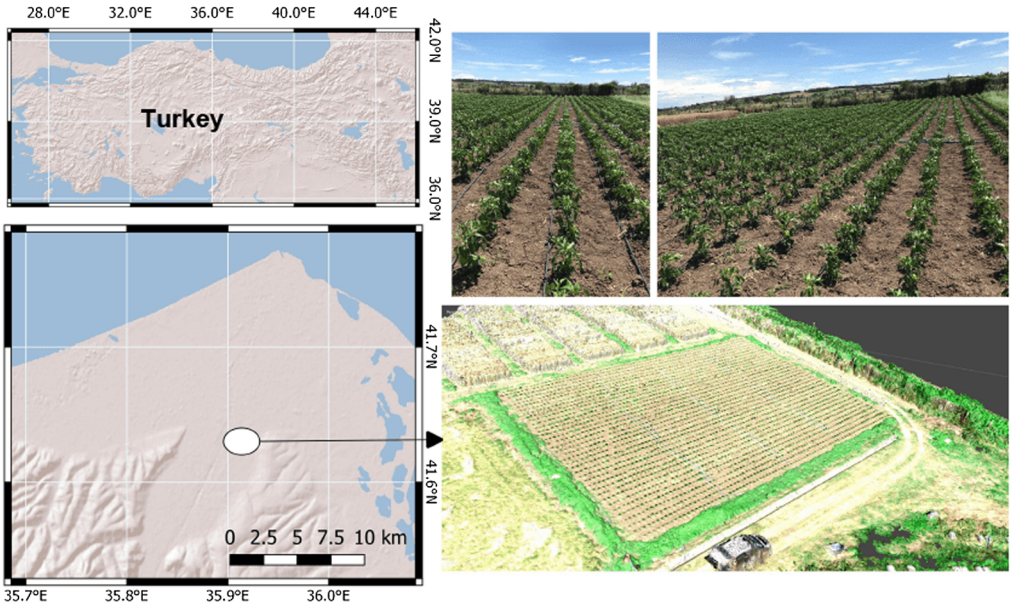

Fig. 1 Bell pepper experiment area at Black Sea Agricultural Research Institute in 2019.

According to long-term climatic data, the annual mean precipitation is 694 mm, the mean maximum air temperature is 27°C in August, and the minimum air temperature is 3.7°C in February. The mean air temperature and relative humidity are 14.4°C and 72.7%, respectively (MGM, 2019).[36] Reference 35 stated that the experimental area's soils were classified as clay in the top 0 to 90 cm and clay-loam from 90 to 120 cm. The storage capacity of the plant available water (PAW) at 0 to 30 cm, 30 to 60 cm, 60 to 90 cm, and 90 to 120 cm depths was 0.142, 0.140, 0.155, and 0.154 $m^3\ m^{-3}$, respectively.

2.2 *Experimental Design and Treatments*

Four water management regimes (full irrigation, S1; S2, 70% of S1; S3, 40% of S1; rain-fed, S4) were applied in this study. A randomized complete block experimental design was used with three replications. The irrigation times of the S1 treatment plots were determined based on soil water measurements, and a management allowable deficit value of 40% was used. Soil water content measurements of all experimental plots were carried out at each 30-cm depth of a 120-cm soil profile throughout the growing season. Irrigation was scheduled based on the soil water depletion within bell pepper's effective rotting depth (60 cm). A 40% depletion of the total available soil water holding capacity was considered the threshold of irrigation timing. Thus, the amounts of irrigation in each water application for the S1 treatment were determined with respect to depth as the difference between field capacity and the soil moisture content measured. The irrigation timing of the S2 and S3 treatments was the same as S1, and the irrigation percentages of the S2 and S3 treatments were 70% and 40% of the S1 treatment, respectively. Crops in the S4 treatment plots were grown under rain-fed conditions. However, to provide appropriate soil moisture conditions for transplanted bell pepper crops, on 16 and 25 days after planting (DAP), a total of 30 mm of irrigation water was applied. After DAP 25, irrigation water was applied to the plots based on experimental treatments, and no irrigation was applied to the S4 plots. Irrigation was applied using a drip irrigation system designed for this trial by considering the soil physical properties, crop spacing, and experimental water applications.

Each trial plot's dimensions were 5.6×7.0 m, and edge effects were considered during each harvest. Thus, each harvest plot was 4.2-m wide (six plant rows) and 4.8-m long with a 2.1-m space between each plot (Fig. 2). Bell pepper seedlings were also transplanted in spaces between the plots to protect experimental crops from the negative effect of micrometeorological events that can occur on bare soil.

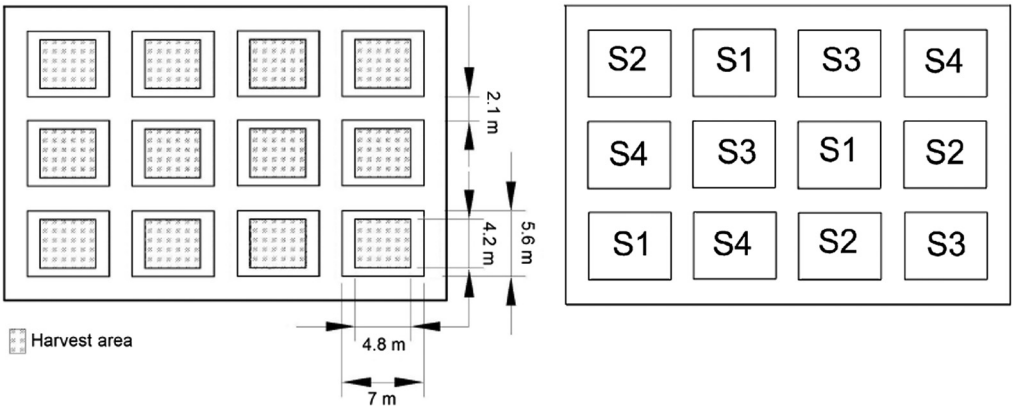

Fig. 2 Experimental design showing the distribution of plots in the study.

2.3 *Soil Water Budget and Crop Evapotranspiration*

The daily reference evapotranspiration (ET_o) was calculated using the FAO Penman–Monteith equation.[37] In addition, each experimental plot's actual evapotranspiration values were calculated based on the soil water budget approach for a period between the two consecutive soil water content measurements. To improve the soil water budget results' accuracy, evapotranspiration of the root zone area ($ET_{a_{rz}}$) and of the entire cultivation area (ET_a) were calculated separately based on the area wetted and percentage of vegetation cover. The procedures to calculate $ET_{a_{rz}}$ and ET_a can be found in Ref. 35.

2.4 *Bell Pepper Agronomy and Yield*

The bell pepper variety used in this study was Kundu F1, which is grown widely in the study region. According to this variety's characteristics, the fruit height is 7 cm and width is 6 cm under ideal growing conditions. Bell pepper (*Capsicum annum L.*) seedlings were transplanted on May 15, 2019, and the plants were grown in 70-cm rows where they were spaced 40 cm apart. Based on the soil chemical analyses results, a total of 0.06 tons ha^{-1} P_2O_5 and 0.03 tons ha^{-1} N fertilizer were applied before transplanting, and 0.1 tons ha^{-1} N fertilizer was applied during the initial and development stages as a five-equal part. While N fertilizer was applied via the drip irrigation system for the S1, S2, and S3 treatments, it was applied equally by hand in the S4 plots. Weeds were controlled using herbicides in the early season, and thereafter, weeding was performed with a hoe.

All mature bell pepper fruits were harvested by handpicking, and a total of six harvests was obtained. Yield and quality parameters, such as fruit height, width, and thickness, were measured after each harvest.

2.5 *UAV System, Flight Planning, and Image Processing*

The DJI S1000+ octocopter with an A2 flight control system (DJI, Shenzhen, China) was used as the UAV in this study. It has a maximum payload capacity of 11 kg and maximum flight duration of 15 min under optimal weather conditions. DJI Datalink was used to connect the ground control system and UAV, and Universal Ground Control Station (UGCS) software was used for mission planning and autonomous flight.

High-resolution multispectral images were obtained from the Micasense Altum (Seattle, Washington, United States) sensors. This camera can capture blue (475 nm), green (560 nm), red (668), RedEdge (717 nm), near-infrared (NIR) (840 nm), and thermal images (8 to 14 μm) simultaneously. The multispectral and thermal sensors' resolution are 5.2 and 81 cm, respectively, 120-m above ground level. This camera has a sunshine sensor to measure downwelling irradiance during the flight. Further, it has a global positioning system (GPS) that obtains location information for each image and has a calibration reflectance panel to calibrate the irradiance value.

The same mission plan with parallel paths was used for each flight, which allowed the UAV system to capture several multispectral images and cover 12 experimental plots. The flight mission was planned at 40 m above ground level at a speed of 2 $\mathrm{m\,s^{-1}}$. To obtain high-quality mosaic images, multispectral imagery was captured with 80% sidelap and overlap. Accordingly, the multispectral camera's image capturing interval and distance between flight paths were calculated based on the UAV's flight height and speed, and specific parameters related to the camera, such as field of view degree, the maximum capture rate per second, and focal length.

Multispectral image sets consisting of five separate spectral bands were obtained. Because each pixel value of these images was acquired as a digital number (DN), raw multispectral pixel values were converted to absolute reflectance values using Eq. (1)

$$L = V(x,y) \times \frac{a_1}{g} \times \frac{p - p_{\mathrm{BL}}}{t_e + a_2 y - a_3 t_e y}, \tag{1}$$

where L is the spectral radiance ($\mathrm{W/m^2/sr/nm}$), $V(x,y)$ is the vignette polynomial function for each pixel, a_1, a_2, and a_3 are the coefficients for the radiometric calibration, g is the sensor gain (stored in metadata), p is the normalized raw image pixel values (DN), p_{BL} is the value of the black level (stored in metadata tag), and t_e is the exposure time.

The radial vignette model was used to correct the radial reduction of brightness from the image's center to the edges. Equation (2) was applied to the radiance images for vignette correction

$$\begin{aligned} I_{\mathrm{corrected}}(x,y) &= \frac{I(x,y)}{k}, \\ k &= 1 + k_0 \times r + k_1 \times r^2 + k_2 \times r^3 + k_3 \times r^4 + k_4 \times r^5 + k_5 \times r^6, \\ r &= \sqrt{(x - c_x)^2 + (y - c_y)^2}, \end{aligned} \tag{2}$$

where $I_{\mathrm{corrected}}(x,y)$ and $I(x,y)$ are the corrected and original image pixel intensity, k is the correction factor, and r is the image pixels' distance from the vignette center. Python 3.6 was used to convert the raw, high-resolution multispectral images to reflectance, remove lens distortions, and for vignette correction. The Python codes used in this study and details of the formulas can be found at https://github.com/micasense/imageprocessing (last accessed May 11, 2020). Agisoft Metashape 1.6.3 was used to create orthomosaic images according to the procedure given by the camera's manufacturer.[38] The workflow, parameters, and settings used to generate dense cloud, digital elevation map (DEM), and orthomosaic images are provided in Table 1.

Table 1 Agisoft Metashape Processing Options.

Workflow	Parameter	Setting
Align photos	Accuracy	High
	Key point limit	40,000
	Tie point limit	4000
Optimize camera alignment	General parameters	Fit *f*, *cx* – *cy*, *k*1, *k*2, *k*3, *b*1, *b*2, *p*1, and *p*2
Build dense cloud	Quality	Medium
	Depth filtering	Aggressive
Build DEM	Type	WGS 84/UTM Zone 36 N (EPSG::32636)
	Source data	Dense cloud
	Interpolation	Extrapolated
Build orthomosaic	Surface	DEM
	Blending mode	Mosaic (default)

Table 2 List of used vegetation indexes in the study to estimate bell pepper yield and their references.

Vegetation index	References
$\text{NDVI} = \frac{(\text{NIR}-\text{Red})}{\text{NIR}+\text{Red}}$	Tucker, 1979[39]
$\text{SAVI} = (1+L) \times \frac{(\text{NIR}-\text{Red})}{(L+\text{NIR}+\text{Red})}$	Huete, 1988[40]
$\text{SR} = \frac{\text{NIR}}{\text{Red}}$	Aparicio et al., 2000[41]
$\text{EVI} = G \times \frac{(\text{NIR}-\text{Red})}{\text{NIR}+(C1*\text{Red}-C2*\text{Blue})+L}$	Liu and Huete, 1995[42]

Where NIR, Red, Blue are the orthomosaic reflectance images, L (set at 0.5) is the soil adjustment factor to reduce soil noise effect,[43] G is the gain factor (G=2.5), and $C1$ (set at 6) and $C2$ (set at 7.5) are the coefficients of aerosol resistance term.

Spectral vegetation indices were calculated using the corrected orthomosaic reflectance images. A summary of the vegetation indices used is given in Table 2.

Agisoft Metashape software was also used to calculate the bell pepper canopy volume. To do so, shapefiles that cover each plot's harvest area were created separately using a polygon drawing tool. In the second step, each experimental plot's canopy volume was determined in which each plot shapefile's lowest elevation height was defined and considered the ground elevation. Thus, for each plot, ground elevation values were calculated separately. Each canopy volume was calculated based on the differences between bell pepper canopy height and a plot's ground elevation. Details of the volume calculations can be found in Ref. 44.

2.6 *Data Analysis*

Correlation analyses were performed among the high-resolution vegetation index maps, canopy volume, and bell pepper yield. According to the correlation coefficient (r), the best time intervals were determined to estimate yield using vegetation indices and the canopy volume. Bell pepper yield estimation models for each spectral vegetation index and canopy volume were developed with regression analysis to estimate yield. The R^2 and the RMSE were used to evaluate these models' performance.

3 Results and Discussion

3.1 *Soil Moisture and Irrigation Water Amount Results*

Bell pepper $\text{ET}_{a_{rz}}$ and (ET_a) findings, amounts of irrigation water applied, amounts of rainfall received, and estimated ET_o values are given in Table 3. Irrigation amounts of 402.2, 299.5, 196.8, and 60.0 mm were applied to S1, S2, S3, and S4, respectively, during the bell pepper growing period. The total ET_o and rainfall values related to the growing season were 547.3 and 174.7 mm, respectively. The seasonal $\text{ET}_{a_{rz}}$ values calculated ranged from 288.8 to 566.7 and the ET_a values ranged from 217.3 to 356.5 mm. Reference 45 reported that bell pepper's seasonal $\text{ET}_{a_{rz}}$ ranged from 309 to 528 mm. In another study, seasonal red pepper $\text{ET}_{a_{rz}}$ values that ranged

Table 3 Total applied amount of irrigation water, total received rainfall, seasonal crop evapotranspiration, and reference evapotranspiration.

Treatment	Irrigation (mm)	Rainfall (mm)	$\text{ET}_{a_{rz}}$ (mm)	ET_a (mm)	ET_o (mm)
S1	402.2	174.7	566.7	356.5	547.3
S2	299.5		462.9	298.2	
S3	196.8		421.2	273.6	
S4	60.0		288.8	217.3	

from 30 to 567 mm were reported.[46] Differences in bell pepper $ET_{a_{rz}}$ values may be attributable to differences in climatic conditions, soil properties, and the technique used to measure evapotranspiration. It can be said that the results of the bell pepper $ET_{a_{rz}}$ values in this study agree with those in previous research.

3.2 *Bell Pepper Yield and Fruit Quality Results*

Bell pepper yields and fruit quality parameters are provided in Table 4. A total of six harvests was carried out during the growing season in 2019. While the first harvest was performed on DAP 46, the last was carried out on DAP 103. The highest and lowest yields were obtained from the S1 and S4 treatments, respectively. Table 4 shows that bell pepper yields ranged from 24.8 to 51.4 tons ha^{-1}, and there were significant differences in the yield values among the irrigation treatments ($p < 0.05$). According to the least significant difference test results, three groups were identified, *a* (S1), *b* (S2), and *c* (S3 and S4). The results of this study highlight that the bell pepper yield was correlated highly with irrigation regimes. These experimental results are consistent with those in previous studies. Reference 47 stated that bell pepper yields could range from 31.76 to 50.72 tons ha^{-1}. Reference 48 reported minimum and maximum bell pepper yield values of 24.5 and 47.5 tons ha^{-1}, respectively. Reference 46 reported that yields ranged from 10.89 to 44.92 tons ha^{-1} in 2009, and 4.47 to 63.64 tons ha^{-1} in 2010 under the Çanakkale, Turkey climate conditions. Reference 49 indicated that water stress has a significant adverse effect on bell pepper yield. Compared with previous studies, different yield values were obtained in this research, which may be attributable to environmental factors, irrigation methods and amounts, bell pepper variety, and other agricultural practices. Bell pepper fruit quality parameters (average width, height, and thickness) are shown in Table 4. As the table shows, the results indicate that the S1 treatment is superior to other irrigation treatments with respect to all fruit quality parameters. In contrast, according to the parameters measured, fruit quality was poorest under the S4 treatment condition. The highest values for fruit width, height, and thickness were 6.14 cm, 7.04 cm, and 3.35 mm, respectively, for S1, and the lowest values were 5.03 cm, 5.69 cm, and 2.58 mm, respectively, for S4. These results are consistent with those in Ref. 50, which reported that bell pepper canopy width ranged from 6.6 to 7.5 cm under full irrigation, whereas Ref. 51 stated that bell pepper fruit thickness varies depending upon the amount of irrigation. This study's findings on fruit thickness are consistent with those in Ref. 51, which also found that the maximum and minimum bell pepper fruit thickness was 3.47 and 2.74 mm, respectively. Generally, these results are similar to those in previous studies.

3.3 *Spectral Vegetation Indices and Canopy Volume Results*

7 UAV flight missions were conducted on different dates (DAP 44, 49, 56, 63, 72, 87, and 103) throughout the bell pepper growing season. The mean NDVI, soil adjusted vegetation index (SAVI), simple ratio (SR), and enhanced vegetation index (EVI) values of each experimental plot were obtained on each flight date. Their graphical change throughout the growing season is shown in Fig. 3, and an example of the maps generated related to spectral vegetation indices associated with DAP 87 is shown in Fig. 4. As Fig. 3 shows, from seedling to DAP 56,

Table 4 Effects of deficit irrigation on bell pepper yield and average fruit size during the growing period.

Irrigation treatments	Yield (tons ha^{-1})	Fruit width (cm)	Fruit height (cm)	Fruit thickness (mm)
S1	51.49	6.14	7.04	3.35
S2	33.21	5.69	6.55	2.87
S3	30.77	5.34	6.10	2.60
S4	24.82	5.03	5.69	2.58

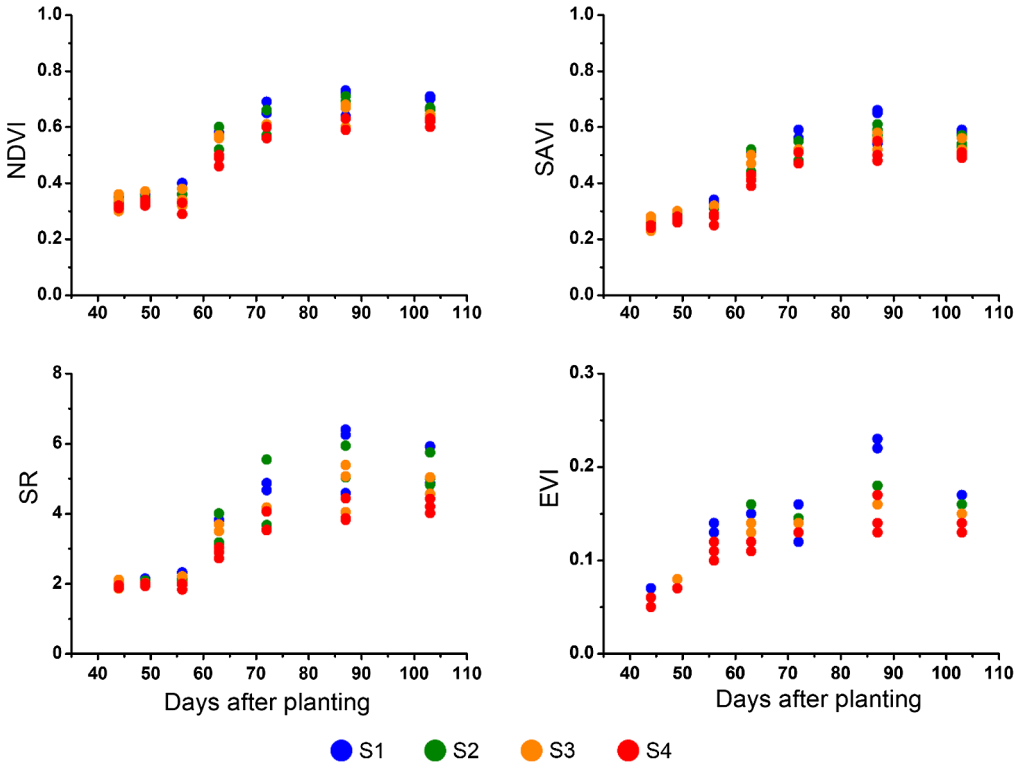

Fig. 3 Changes of vegetation index values in bell pepper experiment plots throughout the growing season.

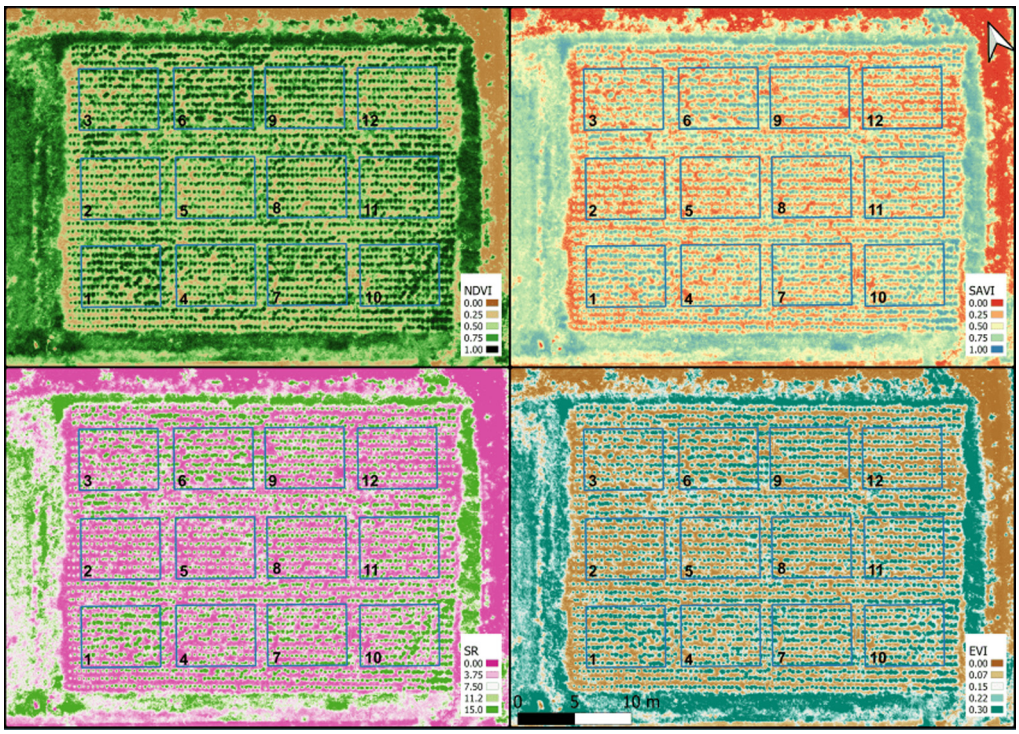

Fig. 4 Bell pepper vegetation index maps were generated from high-resolution multispectral UAV images showing the variation of experimental plots on August 10, 2019 (DAP 87).

no significant differences among plots were found in all vegetation indices. In contrast, all parcels' vegetation index values increased from DAP 63 to 87. Accordingly, the effect of different amounts of irrigation on bell pepper vegetation levels appeared after DAP 63. During the period between DAP 63 and 87, the highest and lowest vegetation index values were found in the S1 and S4 treatment plots, respectively.

Bell pepper NDVI values ranged from 0.23 to 0.79 during the growing season. While the NDVI value peaked on DAP 87, the lowest value was found on DAP 56. Generally, the plots' NDVI values were consistent with the irrigation treatments, and the results agree with those obtained for bell pepper,[52] wheat,[53] green bean,[54] and cotton.[55]

The changes in SAVI during the growing period are shown in Fig. 3. The maximum and minimum SAVI values were 0.66 and 0.23, respectively. These values were calculated on DAP 87 (maximum value) and DAP 44 (minimum value). The full irrigation treatment (S1) had the highest SAVI and NDVI values. Similarly, the lowest SAVI and NDVI values were obtained from the rain-fed S4 treatment. The results showed that different amounts of irrigation lead to different SAVI values in irrigation treatment plots. Reference 56 found that SAVI is correlated highly with crop evapotranspiration ($r = 0.98$).

In this study, the SR values changed from 1.83 to 2.32 between DAP 44 and 63. After DAP 63, the SR values increased and peaked (6.40) on DAP 87. In previous studies,[57] SR was found to be one of the most efficient vegetation indices to monitor different irrigation levels' effect.

Generally, the EVI values among the treatments did not differ significantly until DAP 50. However, from this date to DAP 87, the EVI values increased regularly. The maximum EVI was 0.23 on DAP 87, and the minimum was 0.05 on DAP 44. The maximum and minimum values were obtained from the S1 and S4 treatments, respectively.

Figure 5 shows the bell pepper canopy volumes calculated from UAV images. As shown in Fig. 5, the results indicate that canopy volumes are associated with irrigation treatments. The maximum and minimum volumes were obtained on DAP 103 in plot 1 (S1) and DAP 44 in plot 12 (S4), respectively. Another significant result of this study was that the canopy volumes increased regularly from DAP 44 to 103. This result is consistent with that of Ref. 58, which found that the bell pepper canopy width and height increased with irrigation level and time. In another study conducted in Tarsus, Turkey, bell pepper crop heights were associated with irrigation regimes.[45] On the other hand, the result of this study is inconsistent with that in Ref. 59, which concluded that crop height and irrigation amounts do not differ significantly. This inconsistency may be attributable to different bell pepper growing environments, climate, soil properties, and irrigation practices.

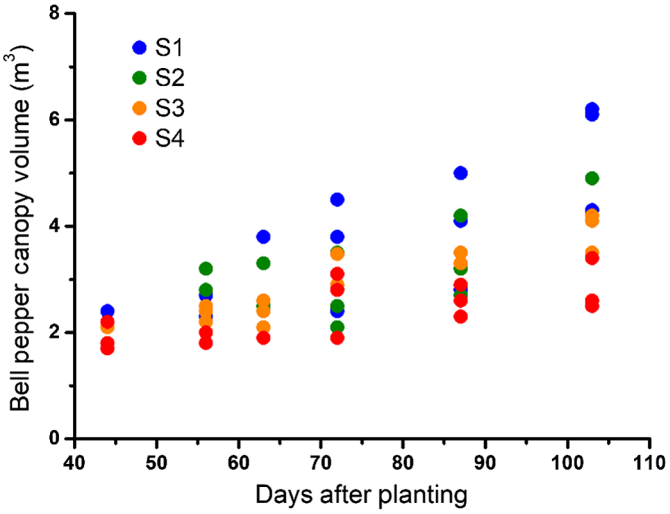

Fig. 5 Variation of bell pepper canopy volume values of all experiment plots at UAV flight campaign days.

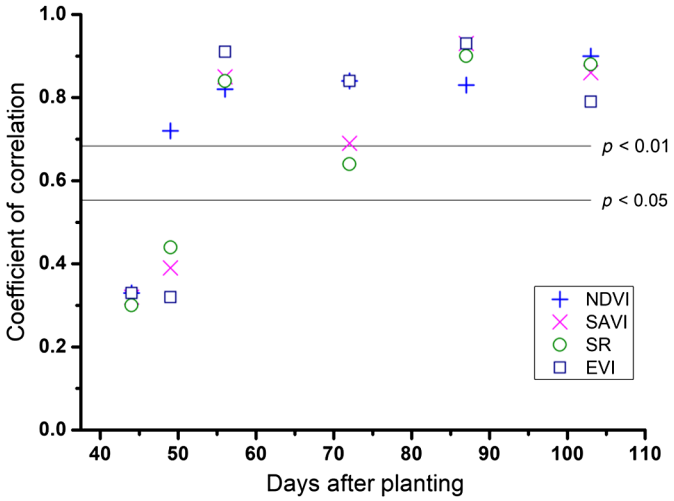

Fig. 6 Changes in correlation coefficients of linear relation between vegetation indexes and bell pepper yield among UAV flight days.

3.4 *Evaluation of Bell Pepper Yield Models*

Statistically significant differences in the correlation coefficient related to a comparison of the vegetation indices and yield throughout the bell pepper growing season are shown in Fig. 6. Further, the summary statistical results of linear regression models developed to estimate bell pepper yield using vegetation indices are given in Table 5.

Table 5 Summary result of regression analysis between vegetation indexes and bell pepper yield values.

	DAP	44	49	56	63	72	87	103
NDVI	*a*	146.7	232.1	263.2	159.2	149.4	160.7	227.4
	b	−14.3	−44.6	−57	−51	−56.8	−72	−116.3
	R^2	0.09	0.13	0.69*	0.59*	0.48*	0.76*	0.76*
	RMSE (tons ha^{-1})	8.5	8.6	4.9	5.6	7.0	4.3	4.5
SAVI	*a*	208.1	288.6	305.9	163.8	159	157	251.3
	b	−19.1	−46.1	−56.3	−40.7	−47.7	−55	−101.6
	R^2	0.1	0.15	0.72*	0.60*	0.48*	0.86*	0.74*
	RMSE (tons ha^{-1})	8.4	8.5	4.7	5.6	7	3.3	4.7
SR	*a*	33.4	71.8	56.5	16.7	9.7	9.3	12.8
	b	−32.3	−110.8	−82.6	−21.7	−6.6	−12.8	−29.9
	R^2	0.09	0.19*	0.71*	0.58*	0.41*	0.81*	0.78*
	RMSE (tons ha^{-1})	8.4	8.7	4.7	5.7	7.4	3.9	4.4
EVI	*a*	874.3	652.7	823.7	434.9	575.8	305.2	607.6
	b	−18.6	−13.5	−62.9	−22.4	−44.1	−18.5	−54.6
	R^2	0.11	0.10	0.82*	0.62*	0.71*	0.87*	0.62*
	RMSE (tons ha^{-1})	8.3	8.4	3.8	5.4	5.3	3.1	5.7

*$p < 0.01$.

The threshold values of the correlation coefficients were 0.68 and 0.55 at $p < 0.01$ and $p < 0.05$, respectively. According to the $p < 0.05$ level, the seasonal bell pepper yield can be estimated after DAP 49 using the NDVI and after 56 using the SAVI, SR, and EVI indices.

NDVI has a more extended yield estimation period than the other vegetation indices. Bell pepper yield can be estimated using NDVI values between DAP 49 and 103 at the $p < 0.01$ significance level. Generally, the error in the bell pepper yield estimation decreased from DAP 49 to 103 when NDVI was used. Thus, the level of success in estimating yield increased as DAP 103 approached. Although the highest correlation between NDVI and yield was found on DAP 103, the lowest RMSE (4.3 tons ha^{-1}) was found on DAP 87.

The SAVI values calculated from high-resolution UAV images between DAP 56 and 103 estimated bell pepper yield successfully at the $p < 0.01$ level. The highest correlation coefficient ($r = 0.93$) was found on DAP 87, and the RMSE value of the estimated yield was 3.3 tons ha^{-1}. The lowest correlation coefficient ($r = 0.32$) was obtained on DAP 44, and was not statistically significant.

Bell pepper yield can be estimated using SR between DAP 49 and 103 at the $p < 0.05$ significance level. At the $p < 0.01$ level, SR can be used to estimate bell pepper yield between DAP 49 and 103, except for DAP 72, which was not significant at $p < 0.01$, but was at $p < 0.05$. The SR's highest and lowest correlation coefficient was 0.90 on DAP 87 and 0.30 on DAP 44, respectively.

Generally, EVI has a higher correlation with estimates of bell pepper yield than the other vegetation indices. The bell pepper yield could be estimated with minimum estimation error (RMSE = 3.2 tons ha^{-1}) using EVI on DAP 87. The regression analysis between yield and the EVI value on DAP 87 had an R^2 of 0.81 ($p < 0.01$).

This study found that vegetation indices (NDVI, SAVI, SR, and EVI) can be used to estimate bell pepper yield between DAP 56 and 103. These results reflect those of Ref. 60, in which a field experiment was conducted to monitor bell pepper vegetation using a spectroradiometer under different irrigation conditions. The authors concluded that SR can be used successfully to estimate bell pepper yield ($r = 0.90$). According to Ref. 17, sunflower yield is correlated highly with the NDVI values calculated from UAV images. In another study, pasture yield was estimated using the NDVI and SR that were calculated from high-resolution UAV images,[61] while Ref. 62 reported that EVI can be used to estimate soybean yield.

The results of the correlation analysis between the bell pepper canopy volume and yield are given in Table 6. From the data, it is apparent that the correlation coefficient values increased from DAP 44 to 103. The highest and lowest correlation coefficients were 0.97 on DAP 103 and 0.32 on DAP 56. On DAP 103, there was a significant linear relation between the canopy volume and yield values with a R^2 value of 0.93 ($p < 0.01$, Fig. 7). The RMSE value of this yield estimation was 2.3 tons ha^{-1}. These results are consistent with those obtained by Ref. 63, which found a high correlation ($r = 0.88$) between orange yield and canopy volume and Ref. 64, which

Table 6 Summary result of regression analysis between bell pepper canopy volume and yield values.

	DAP	44	49	63	72	87	103
Bell pepper canopy volume	*a*	15.41	7.21	11.93	9.56	10.43	7.66
	b	2.05	17.08	4.35	5.44	−0.04	2.46
	R^2	0.12	0.10	0.73	0.58	0.81	0.93
	RMSE (tons ha^{-1})	8.3	8.3	8.1	5.7	3.8	2.3
	Coefficient of correlation	0.35	0.32	0.85*	0.76*	0.90*	0.97*

*$p < 0.01$.

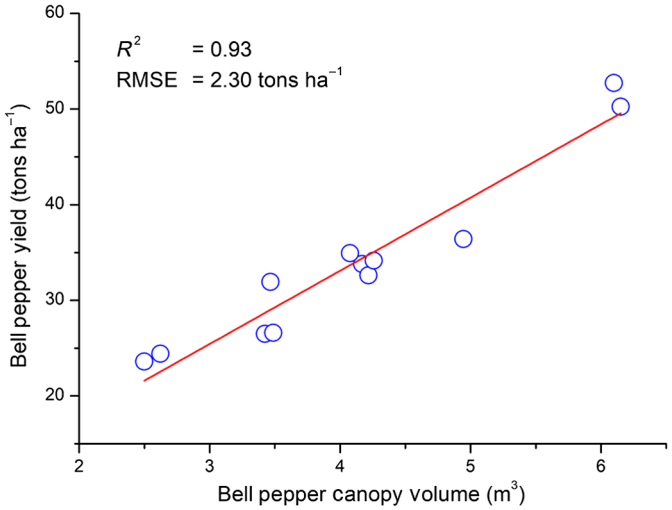

Fig. 7 Linear relation between bell pepper canopy volume values calculated from UAV images acquired on DAP 103 and bell pepper yield of 12 experiment plots.

used a light detection and ranging sensor to calculate walnut tree canopy volume and reported that there was a linear relation between tree volume and yield ($R^2 = 0.77$).

4 Conclusion

In this study, bell pepper yield was estimated with NDVI, SAVI, SR, EVI, and canopy volume. UAV images were acquired on seven dates between DAP 44 and 103 at 40-m above ground level with a 2-cm spatial resolution. A linear regression analysis was performed between the yield and vegetation indices. The regression analysis results showed that bell pepper yield can be estimated using the vegetation index between DAP 56 and 103 at a significance level of 0.01. EVI was the best vegetation index to estimate yield with the minimum estimation error among the vegetation indices. According to the results of this study, bell pepper yield can be estimated on DAP 87 using the equation of yield $= 305.2\text{EVI} - 18.54$ to generate yield maps. These maps can help farmers to estimate bell pepper yield during the growing season, and contribute to evaluating agricultural practices to obtain the maximum yield. Further, policymakers can use yield maps to balance market prices, and they also have considerable potential for use in the agricultural insurance sector.

The relation between bell pepper yield and canopy volume was examined in this study. The results showed that yield estimation error decreased near DAP 103. The result of the regression analysis between canopy volume and yield on DAP 87 showed that the highest R^2 was 0.93 and the lowest RMSE was 2.1 tons ha^{-1}. In general, canopy volumes performed better than vegetation indices to estimate yield, which indicates that bell pepper canopy volumes can be used successfully to estimate yield. While calculating canopy volume is difficult, time-consuming, and tedious in field conditions, high-resolution UAV images can be used to do so rapidly, precisely, and at lower cost.

This study was one of the first attempts to examine bell pepper yield estimation thoroughly using high-resolution vegetation index maps and canopy volumes. More research is needed to understand the relation between yield and vegetation indices/canopy volume better. Thus, further research under controlled experimental conditions is recommended in different climatic conditions and with other crops. Moreover, studies are needed on multispectral sensor quality, flight altitude, and timing.

Acknowledgments

This study was supported by the Ondokuz Mayıs University (PYO.ZRT.1904.19.001).

References

1. M. K. Bozokalfa and D. Eşiyok, "Genetic diversity in pepper (*Capsicum annuum L.*) accessions as revealed by agronomic traits," *Ege Üniversitesi Ziraat Fakültesi Dergisi* **47**(2), 123–134 (2010).
2. A. Marques, Jr. et al., "Statistical assessment of cartographic product from photogrammetry and fixed-wing UAV acquisition," *Eur. J. Remote Sens.* **53**(1), 27–39 (2020).
3. H. Govil et al., "Identification of new base metal mineralization in Kumaon Himalaya, India, using hyperspectral remote sensing and hydrothermal alteration," *Ore Geol. Rev.* **92**, 271–283 (2018).
4. C. Echappé et al., "Satellite remote sensing reveals a positive impact of living oyster reefs on microalgal biofilm development," *Biogeosciences* **15**(3), 905–918 (2018).
5. J.-I. Shin et al., "Using UAV multispectral images for classification of forest burn severity—A case study of the 2019 Gangneung forest fire," *Forests* **10**(11), 1025 (2019).
6. V. Novák and K. Křížová, "Sentinel-2 imagery utilization for small-plot agricultural studies," *IOP Conf. Ser. Mater. Sci. Eng.* **725**, 012078 (2020).
7. B. Stevens et al., "Canopy cover evolution, diurnal patterns and leaf area index relationships in a Mchare and Cavendish banana cultivar under different soil moisture regimes," *Sci. Horticulturae* **272**, 109328 (2020).
8. M. Reynolds et al., "EExploring genetic resources to increase adaptation of wheat to climate change," in *Advances in Wheat Genetics: From Genome to Field*, Y. Ogihara, S. Takumi, and H. Handa, Eds., pp. 355–368, Springer, Tokyo (2015).
9. V. Poenaru et al., "Monitoring vegetation phenology in the Braila Plain using Sentinel-2 data," *Sci. Pap. Ser. E* **6**, 175–180 (2017).
10. H. Nieto et al., "Evaluation of TSEB turbulent fluxes using different methods for the retrieval of soil and canopy component temperatures from UAV thermal and multispectral imagery," *Irrigation Sci.* **37**(3), 389–406 (2019).
11. D. Belton et al., "Crop height monitoring using a consumer-grade camera and UAV technology," *PFG–J. Photogramm. Remote Sens. Geoinf. Sci.* **87**(5), 249–262 (2019).
12. C. L. Doughty and K. C. Cavanaugh, "Mapping coastal wetland biomass from high resolution unmanned aerial vehicle (UAV) imagery," *Remote Sens.* **11**(5), 540 (2019).
13. A. Feng et al., "Yield estimation in cotton using UAV-based multi-sensor imagery," *Biosyst. Eng.* **193**, 101–114 (2020).
14. J. Ren et al., "Regional yield estimation for winter wheat with MODIS-NDVI data in Shandong, China," *Int. J. Appl. Earth Obs. Geoinf.* **10**(4), 403–413 (2008).
15. V. Dadhwal and S. Ray, "Crop assessment using remote sensing-Part II: crop condition and yield assessment," *Indian J. Agric. Econ.* **55**, 55–67 (2000).
16. K. R. Thorp et al., "Methodology for the use of DSSAT models for precision agriculture decision support," *Comput. Electron. Agric.* **64**(2), 276–285 (2008).
17. E. Tunca et al., "Yield and leaf area index estimations for sunflower plants using unmanned aerial vehicle images," *Environ. Monit. Assess.* **190**(11), 682 (2018).
18. M. L. Hunt et al., "High resolution wheat yield mapping using Sentinel-2," *Remote Sens. Environ.* **233**, 111410 (2019).
19. S. Olanrewaju et al., "Using aerial imagery and digital photography to monitor growth and yield in winter wheat," *Int. J. Remote Sens.* **40**(18), 6905–6929 (2019).
20. S. D. Durgan and C. Zhang, "Unmanned aircraft system (UAS) for wetland species mapping," in *Multi-Sensor System Applications in the Everglades Ecosystem*, Q. Wheng, Ed., pp. 89–108, CRC Press, Boca Raton, Florida (2020).
21. J. A. Berni et al., "Thermal and narrowband multispectral remote sensing for vegetation monitoring from an unmanned aerial vehicle," *IEEE Trans. Geosci. Remote Sens.* **47**(3), 722–738 (2009).
22. S. G. Gupta, D. Ghonge, and P. M. Jawandhiya, "Review of unmanned aircraft system (UAS)," *Int. J. Adv. Res. Comput. Eng. Technol.* **2**, 1646 (2013).
23. A. Matese et al., "Estimation of water stress in grapevines using proximal and remote sensing methods," *Remote Sens.* **10**(1), 114–114 (2018).

24. J. Sarron et al., "Mango yield mapping at the orchard scale based on tree structure and land cover assessed by UAV," *Remote Sens.* **10**(12), 1900 (2018).
25. B. Duan et al., "Remote estimation of rice yield with unmanned aerial vehicle (UAV) data and spectral mixture analysis," *Front. Plant. Sci.* **10**, 204 (2019).
26. S. F. Di Gennaro et al., "A low-cost and unsupervised image recognition methodology for yield estimation in a vineyard," *Front. Plant. Sci.* **10**, 559 (2019).
27. M. Zhang et al., "Estimation of maize yield and effects of variable-rate nitrogen application using UAV-based RGB imagery," *Biosyst. Eng.* **189**, 24–35 (2020).
28. L. Shi, S. Hu, and Y. Zha, "Estimation of sugarcane yield by assimilating UAV and ground measurements via ensemble Kalman filter," in *IEEE Int. Geosci. and Remote Sens. Symp.*, pp. 8816–8819 (2018).
29. M. Maimaitijiang et al., "Soybean yield prediction from UAV using multimodal data fusion and deep learning," *Remote Sens. Environ.* **237**, 111599 (2020).
30. H. Escalante et al., "Barley yield and fertilization analysis from UAV imagery: a deep learning approach," *Int. J. Remote Sens.* **40**(7), 2493–2516 (2019).
31. Y. Gong et al., "Remote estimation of rapeseed yield with unmanned aerial vehicle (UAV) imaging and spectral mixture analysis," *Plant Methods* **14**(1), 70 (2018).
32. B. Li et al., "Above-ground biomass estimation and yield prediction in potato by using UAV-based RGB and hyperspectral imaging," *ISPRS J. Photogramm. Remote Sens.* **162**, 161–172 (2020).
33. D. Yu et al., "Improvement of sugarcane yield estimation by assimilating UAV-derived plant height observations," *Eur. J. Agron.* **121**, 126159 (2020).
34. Y. Song et al., "Using UAV-based SOPC derived LAI and SAFY model for biomass and yield estimation of winter wheat," *Remote Sens.* **12**(15), 2378 (2020).
35. E. S. Köksal et al., "Evaluation of financial efficiency of drip-irrigation of red pepper based on evapotranspiration calculated using an iterative soil water-budget approach," *Scientia Horticulturae* **226**, 398–405 (2017).
36. MGM, "Turkish State Meteorological Service," 2019, https://mgm.gov.tr/.
37. R. G. Allen et al., "Crop evapotranspiration-guidelines for computing crop water requirements-FAO irrigation and drainage paper 56," FAO, Rome (1998).
38. L. Agisoft, "Agisoft Metashape. St. Petersburg, Russia," 2020, https://agisoft.freshdesk.com/support/solutions/articles/31000148381-micasense-altum-processing-workflow-including-reflectance-calibration-in-agisoft-metashape-professi.
39. C. J. Tucker, "Red and photographic infrared linear combinations for monitoring vegetation," *Remote Sens. Environ.* **8**(2), 127–150 (1979).
40. A. R. Huete, "A soil-adjusted vegetation index (SAVI)," *Remote Sens. Environ.* **25**(3), 295–309 (1988).
41. N. Aparicio et al., "Spectral vegetation indices as nondestructive tools for determining durum wheat yield," *Agron. J.* **92**(1), 83–91 (2000).
42. H. Q. Liu and A. R. Huete, "A feedback based modification of the NDVI to minimize canopy background and atmospheric noise," *IEEE Trans. Geosci. Remote Sens.* **33**(2), 457–465 (1995).
43. R. G. Allen, M. Tasumi, and R. Trezza, "Satellite-based energy balance for mapping evapotranspiration with internalized calibration (METRIC)—Model," *J. Irrig. Drain. Eng.* **133**(4), 380–394 (2007).
44. L. Agisoft, *Agisoft Photoscan User Manual*, Professional Edition, Agisoft LLC., St Petersburg, Russia (2014).
45. S. M. Sezen, A. Yazar, and S. Eker, "Effect of drip irrigation regimes on yield and quality of field grown bell pepper," *Agric. Water Manage.* **81**(1-2), 115–131 (2006).
46. K. Demirel et al., "Effects of different irrigation levels on pepper *Capsicum annum* cv. kapija) yield and quality parameters in semi-arid conditions," *Tekirdağ Ziraat Fakültesi Dergisi* **9**(2), 7–15 (2012).
47. S. Ergün, "Studies on the effects of different irrigation water applications on yield and quality of 'Yalova Corbaci-12' pepper variety in Yalova climate conditions," Atatürk Bahçe Kültürleri Merkez Araştırma Enst., Yalova (1994).

48. H. Kırnak, C. Kaya, and V. Değirmenci, "Growth and yield parameters of bell peppers with surface and subsurface drip irrigation systems under different irrigation levels," *Atatürk Üniversitesi Ziraat Fakültesi Dergisi* **33**(4), 383–389 (2002).
49. L. D. Costa and G. Gianquinto, "Water stress and watertable depth influence yield, water use efficiency, and nitrogen recovery in bell pepper: lysimeter studies," *Aust. J. Agric. Res.* **53**(2), 201–210 (2002).
50. P. A. Rocha et al., "Bell pepper cultivation under different irrigation strategies in soil with and without mulching," *Horticultura Brasileira* **36**(4), 453–460 (2018).
51. A. Abdelkhalik et al., "Effects of deficit irrigation on the yield and irrigation water use efficiency of drip-irrigated sweet pepper (*Capsicum annuum* L.) under Mediterranean conditions," *Irrigation Sci.* **38**(1), 89–104 (2020).
52. S. O. Ihuoma and C. A. Madramootoo, "Crop reflectance indices for mapping water stress in greenhouse grown bell pepper," *Agric. Water Manage* **219**, 49–58 (2019).
53. M. A. Hassan et al., "A rapid monitoring of NDVI across the wheat growth cycle for grain yield prediction using a multi-spectral UAV platform," *Plant Sci.* **282**, 95–103 (2019).
54. E. S. Köksal et al., "Estimation of green bean yield, water deficiency and productivity using spectral indexes during the growing season," *Irrigation Drainage Syst.* **22**(3-4), 209–223 (2008).
55. A. Attia and N. Rajan, "Within-season growth and spectral reflectance of cotton and their relation to lint yield," *Crop Sci.* **56**(5), 2688–2701 (2016).
56. E. S. Köksal, "Hyperspectral reflectance data processing through cluster and principal component analysis for estimating irrigation and yield related indicators," *Agric. Water Manage.* **98**(8), 1317–1328 (2011).
57. Y. Peng and A. A. Gitelson, "Remote estimation of gross primary productivity in soybean and maize based on total crop chlorophyll content," *Remote Sens. Environ.* **117**, 440–448 (2012).
58. T. Gadissa and D. Chemeda, "Effects of drip irrigation levels and planting methods on yield and yield components of green pepper (*Capsicum annuum* L.) in Bako, Ethiopia," *Agric. Water Manage* **96**(11), 1673–1678 (2009).
59. Á. H. C. de Souza et al., "Response of bell pepper to water replacement levels and irrigation times," *Pesquisa Agropecuária Trop.* **49**, 1–7 (2019).
60. K. Demirel et al., "Yield estimate using spectral indices in eggplant and bell pepper grown under deficit irrigation," *Fresenius Environ. Bull.* **23**(5), 1232–1237 (2014).
61. M. Aboutalebi, A. F. Torres-Rua, and N. Allen, "Multispectral remote sensing for yield estimation using high-resolution imagery from an unmanned aerial vehicle," *Proc. SPIE* **10664**, 106640K (2018).
62. G. K. D. A. Figueiredo et al., "Correlation maps to assess soybean yield from EVI data in Paraná State, Brazil," *Scientia Agricola* **73**(5), 462–470 (2016).
63. L. Albrigo et al., "Yield estimation of 'Valencia' orange research plots and groves," *Proc. Fla. State Hort. Soc.*, pp. 44–49 (1975).
64. J. P. Underwood et al., "Mapping almond orchard canopy volume, flowers, fruit and yield using lidar and vision sensors," *Comput. Electron. Agric.* **130**, 83–96 (2016).

Emre Tunca received his engineering degree in agriculture from Ondokuz Mayıs University, Turkey, in 2012. He is currently working as a research assistant at the Ondokuz Mayıs University. His research interests include vegetation monitoring and evapotranspiration mapping.

Eyüp Selim Köksal graduated from Uludağ University. He received his PhD in the Department of Agricultural Structures and Irrigation, Agriculture Faculty, Ankara University in 2006. Currently, he is a professor at the Ondokuz Mayıs University. His research interests include optical and thermal RS, land surface energy balance, and irrigation water management.